Proceedings of Montreal 2018
Global Power and Propulsion Forum
7th - 9th May, 2018
www.gpps.global

GPPS-NA-2018-0105

ON THE NUMERICAL SIMULATION OF SURGE CYCLES USING A QUASI-UNSTEADY MIXING-PLANE APPROACH

Kai Becker

German Aerospace Center (DLR)
Kai.Becker@dlr.de
Linder Höhe, D-51147 Cologne, Germany

Benedict Geihe

German Aerospace Center (DLR)
Benedict.Geihe@dlr.de
Linder Höhe, D-51147 Cologne, Germany

Graham Ashcroft

German Aerospace Center (DLR)
Graham.Ashcroft@dlr.de
Linder Höhe, D-51147 Cologne, Germany

Harald Schoenenborn

MTU Aero Engines AG
Harald.Schoenenborn@mtu.de
Dachauer Str. 665, D-80995 Munich, Germany

ABSTRACT

For future high-pressure compressors, advanced blade designs have to be developed to meet the higher loads. In particular the flow breakdown during surge cycles is a challenging problem for the blades. Furthermore, the prediction of the real loads during the reverse flow is essential for the design of thin trailing edges. In this paper a numerical setup is described to simulate the surge cycle using an unsteady mixing-plane and the control mechanism of the boundary conditions. Its basic aspects are verified using academic test cases. The potential of the concept is demonstrated with a scaled multi-stage compressor. The results are compared with data obtained from a more standard fully unsteady time-domain simulation.

INTRODUCTION

In the development of modern aircraft engines, numerical flow simulations have become indispensable. To further increase efficiency, lower weight and reduce the overall number of engine parts increasingly robust, accurate and well validated numerical methods are required in the design process. The demands on the computational simulation have therefore increased considerably as it has become necessary to exploit design details to push the boundaries of technical limits.

Future high-pressure compressors involve a higher total pressure ratio (> 60) at a smaller core engine with a higher number of stages. Advanced designs have to be developed for leakage reducing adjustable stages, blisks with a short structural length (high aspect ratios) as well as thin and robust vane trailing edges to build highly efficient compressors. One key issue in the design of thin trailing edges is the prediction of loads during surge cycles. During surge cycles the flow breaks down completely in the compressor. This is aerodynamically and mechanically undesirable since parts of the rotor can be damaged and the whole cycle operation may be affected. Furthermore, it results in high temperatures, high levels of vibration and leads to flow reversal. The prediction of blade loads during surge is still a challenging task.

The compressor surge comprises four phases, the pressure rise, the flow breakdown, the blow-down and the flow recovery. Usually, blade loadings during surge are often referred to as surge loads, suggesting that there is a single source of blade loading. In the paper of Schoenenborn and Breuer (2011) the surge load was found to comprise two physically different mechanisms, a pressure shock due to the pressure breakdown and an aeroelastic excitation during the blow-down phase. During the blow-down phase reversed flow conditions exist where a blade may accumulate hundreds of vibration cycles depending on the surge volume and the vibration frequency. High vibration amplitudes and blade damages were observed in the past (Schoenenborn and de Vries, 2012). During surge cycles the loading of the blades changes from stall to reversed flow very quickly (di Mare et al., 2009). The blades suffer a mechanical shock whose extent should be well known for the blade design. Therefore, it is necessary to calculate 3D aerodynamic damping under surge conditions requiring 3D unsteady RANS computations.

One key issue for these simulations is the appropriate propagation of the boundary conditions at compressor inlet and outlet throughout the complete cycle. At the inlet distributions for the absolute total pressure, the absolute total temperature and the flow angles are usually specified whereas the

static pressure is set at the outlet taking into account the radial equilibrium.

Near stall, it becomes difficult to obtain reliable data for the inlet boundary conditions. During the blow-down phase the flow might even reverse itself so that the inlet would become the actual outlet. As a solution Vahdati et al. (2006) proposed to consider the upstream engine parts in the simulation. Therefore, they included the low pressure compressor and the intake in their 3D viscous time-accurate flow analysis of a surge event of a complete core compressor and used far field atmospheric boundary conditions. Downstream of the compressor they placed a variable nozzle controlling the operating point with a change of the nozzle area. Hence, the solution was independent of the prescribed boundary condition at the nozzle exit. Di Mare et al. (2009) added even the combustion chamber to their numerical model.

More recently coupling methods between 3D and 1D CFD solvers were presented to compute the unsteady aerodynamic flow of a compressor during a surge cycle (de Crécy et al., 2013; Dumas et al., 2015). The main idea here is to reduce the computational cost in comparison to the previous described methods. During the 3D URANS computation the inlet and outlet boundary conditions of the compressor are updated dynamically with the results of the coupled 1D solver. The 1D solver comprises the compressor and the adjacent components of the engine like the combustion chamber and the nozzle guide vane of the turbine.

The aim of the current paper is to demonstrate the ability of the CFD solver TRACE to model surge cycles without user interaction. Two methods are introduced to control the static pressure at the system outlet. In the first method the value is simply varied for the different phases. In the second approach a variable convergent-divergent nozzle is placed at the system exit resulting in a supercritical outflow. The operating point is controlled by the narrowest cross section of the nozzle. In the following section a brief overview of the underlying flow solver and the concept of the unsteady mixing-plane is presented. The basic control concepts for the surge cycle are then described in more detail before being verified with two academic test cases. Finally, the methods are applied to simulate the time-periodic flow in a scaled axial compressor rig.

NUMERICAL METHODS

The numerical simulations performed in this work are carried out using the CFD code TRACE (Becker et al., 2010). TRACE is a parallel Navier-Stokes flow solver for structured and unstructured grids that has been developed at DLR's Institute of Propulsion Technology in Cologne to model and investigate turbomachinery flows. The code solves the compressible Reynolds-Averaged Navier-Stokes (RANS) equations in the relative frame of reference using the finite volume method. Inviscid fluxes are evaluated using Roe's flux-difference-splitting method with the upwind states computed using the MUSCL family of schemes in conjunction with a modified van Albada limiter to avoid unphysical oscillations in the vicinity of shocks (Kügeler et al., 2008). Viscous terms are discretized using second-order accurate central differences. Furthermore, it has a wide variety of models adapted for turbomachinery flows. For the effects of turbulence the two-equation Wilcox 1988 $k-\omega$ model (Wilcox, 1988), with extensions for streamline curvature and rotation, compressibility and the suppression of the so-called stagnation point anomaly (Franke et al., 2010), is employed in all Navier-Stokes simulations presented in this work. For time-domain simulations both conventional and higher-order accurate time-integration schemes are available (Ashcroft et al., 2013). The aeroelastic analysis, both flutter and forced response problems, is carried out using a mapping algorithm developed to map structural eigenmodes (Voigt et al., 2010). Using deformation vectors for each cells and a scalar displacement factor the current geometry is constructed. In this work this concept is adapted to create a variable nozzle to control the operating point.

Unsteady Mixing-Plane

Fully developed surge can be approximated as a one-dimensional phenomenon with an unsteady, but circumferentially uniform and annulus averaged, mass flow (Vahdati et al., 2006). In the current work, this approximation, along with the neglect of blade row interaction effects, is exploited to compute the time-dependent surge flow in a multistage compressor without the need to resolve the full annulus in the computational domain. To capture and include the time-dependent surge flow, but suppress unsteady blade row interaction effects, a quasi-unsteady mixing-plane approach is adopted. In contrast to conventional mixing-plane approaches used in steady-state simulations, *instantaneous*, circumferentially averaged flow quantities are communicated between blade rows in this approach, rather than the time-mean values. By using circumferentially averaged flow quantities the direct unsteady blade row interaction effects are suppressed. Blade count ratios therefore do not need to be accounted for in simulations. It is sufficient to resolve a single passage per blade row in the computational domain. Furthermore, the suppression of the unsteady blade row interaction effects allows the time-step size to be selected based on the time-scale of the surge cycle rather than the blade or vane passing frequencies, which are typically orders of magnitude higher. The use of *instantaneous*, circumferentially averaged flow quantities on the other hand allows the temporal development of the surge cycle to be included. In this way the developed approach allows surge cycles to be computed at a fraction of the cost of fully unsteady simulations.

Surge Cycle

The applied setup is illustrated in Fig. 1. A large plenum for the intake and the surrounding air is placed in front of the compressor allowing a large bypass ratio of 10 or higher and colored green. The global entry should not be disturbed even under reversed flow conditions. A simplified model of the combustion chamber, illustrated in orange, is positioned aft of the compressor. Since these parts do not contain any vanes and their periodicity can be arbitrarily selected the pitches of these additional volumes are adjusted always to their adjacent

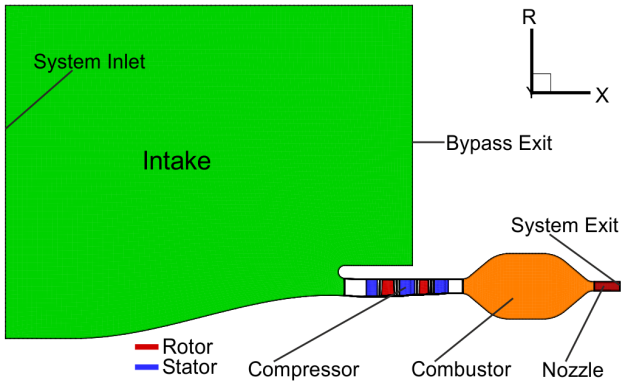

Figure 1. Computational Model For The Surge Cycle.

blade rows. Therefore, zonal interfaces can be used in the simulation at these interfaces to enhance the overall robustness in the calculation. The computational effort for these additional volumes can be neglected in comparison to the number of cells used to mesh the entire compressor. In this approach the system inlet and the system outlet will always remain inlet and outlet respectively. Thus, the standard boundary condition of TRACE can be used here. Additionally, the conditions at the inlet and the outlet of the compressor are self-regulated throughout the simulation. In coupled approaches they would have to be updated continuously by the data of the 1D solver to map the complete surge cycle.

Currently the area of interfaces including inlet and outlet planes cannot be varied during the computation in TRACE. Therefore, it is not possible to use the outlet plane as a choked throttle area to move the compressor towards the surge boundary. So a change in pressure at the outlet of the compressor is provoked either by a change in the exit pressure at the system outlet directly or by the variation of the cross section of a supercritically flowed nozzle located downstream of the combustion chamber. A slight rise in the exit pressure above the last stable operating point is enough to initiate the surge cycle.

The shape of the nozzle is treated as a deformation mode in TRACE so that its cross-section can be modified during the computation. The deformation module was added to the solver for the use in aeroealsticity analysis. Here the displacement of the deformation is either prescribed or based on trigonometric functions and the deformation is recomputed for every time step. For the surge cycle however the displacement has to follow a step function allowing the cross-section to shift between two settings as seen in Fig. 2b. Most of the time the deformation is not altered. Therefore, a general method to describe the displacement was implemented including an algorithm to distinguish between active phases with an actual change of the displacement and passive periods in which the displacement is kept constant to reduce the computational costs.

In the highlighted modification phases the transfer function can be either a straight line or a hyperbolic tangent function. For an easier distinction the settings for the high pressure phase and the low pressure phase are tagged with throttle and release in the results respectively. The shifting is initiated by specified flow conditions at a specific interface of the compressor. In Fig. 2 mass flow criteria are applied. If the mass flow at the compressor inlet becomes negative the settings for the release phase are initiated, marked by the green star. If the mass flow has recovered sufficiently the throttle settings are applied again indicated by the red star. If it is necessary the triggers can be overwritten by the explicitly set times for the related phases.

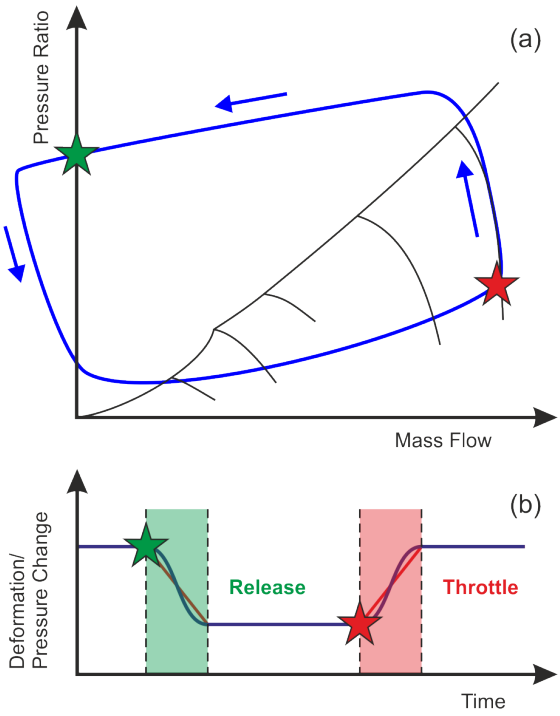

Figure 2. Principles Of The Surge Cycle: (a) Compressor Map with Surge Cycle, (b) Exit Pressure/Deformation over Time.

RESULTS AND DISCUSSION

Before starting the surge cycle computations of a compressor configuration the implementations of the transient mixing-plane and the surge cycle control have to be validated first. Two duct test cases were set up for this purpose.

Verification Of The Unsteady Mixing-Plane

To verify the basic implementation of the transient mixing-plane approach the advection of entropy waves in a uniform subsonic flow across an interface (mixing-plane) between two block groups (one moving, one stationary) is computed by solving the two-dimensional Euler equations on a uniform, structured grid (Fig. 3). At the entry of the computational domain average values of $p_{tot,abs} = 127,000\,Pa$ and $T_{tot,abs} = 342\,K$ are given for the absolute total pressure and the absolute total temperature, respectively. The static pressure at the exit is set to $p = 100,000\,Pa$. Using the gust boundary conditions different entropy waves are prescribed at the inlet. Their propagation is observed when passing the interface. For the unsteady computations a third order accurate implicit Runge Kutta scheme with 32 time steps per period is selected.

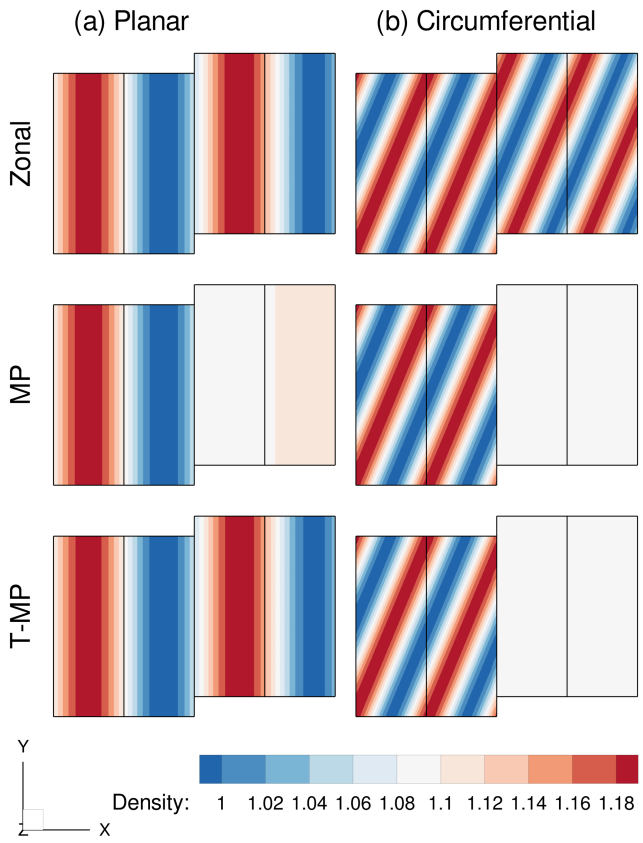

Figure 3. Contour Plots Of The Density Comparing The Three Interface Types For Different Entropy Waves: (a) Planar Wave, (b) Circumferential Wave.

The computations are run for four periods each.

Three different interface types are available: the zonal approach (Zonal), the standard mixing-plane (MP) and the transient mixing-plane (T-MP). The zonal interface is used as a reference for the transient mixing-plane since all waves should pass this interface type without interference. The standard mixing-plane uses time- and circumferentially averaged values. Thus, all waves will be averaged out. The transient mixing-plane approach uses instantaneous, circumferentially averaged values and therefore should be transparent to one-dimensional waves and average out only higher dimensional wave components.

In Fig. 3a, planar waves are discussed. The entropy waves pass the zonal interface (Zonal) without any disturbances. The entropy waves are advected with the underlying subsonic flow normal to the interface. So in the case of the unsteady mixing-plane (T-MP) these waves pass the interface undisturbed. For the standard mixing-plane (MP) balances the waves disappear at the interface as expected. The circumferential waves, described in Fig. 3b, do not possess an axial component. So for both mixing-plane types, MP and T-MP, the waves dissapear. The zonal interface does not influence the propagation of the waves. For the third setup, illustrated in Fig. 4, the planar wave and the circumferential wave are superimposed. As expected the planar waves pass the transient mixing-plane undisturbedly whereas the circumferential

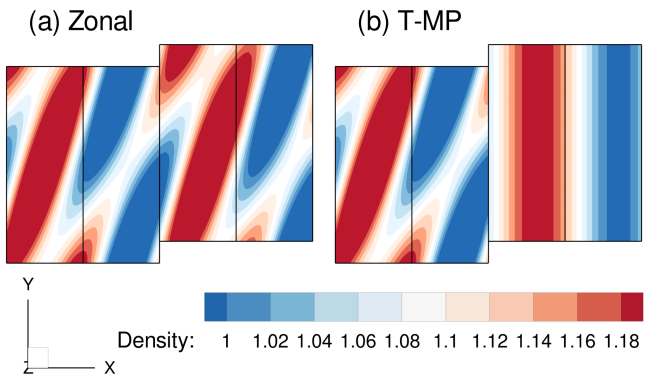

Figure 4. Contour Plots Of The Density For Superimposed Entropy Waves: (a) Zonal, (b) Transient Mixing-Plane.

waves are leveled out in Fig. 4b in contrast to the computation using the zonal interface (Fig. 4a). The computations with the transient mixing-plane produce the expected results. Therefore, it can be stated that the approach is implemented correctly in TRACE.

Prove Of The Nozzle Concept

For the prove of concept of the supercritical nozzle a rotational, non-rotating duct segment is chosen. Starting from constant radii of the hub line and the tip line the deformation module of the TRACE pre-processor PREP is used to create a convergent-divergent nozzle as shown in Fig. 5. The red mesh marks the full deformation of the created eigenmode. The deformation works in the middle part of the duct only so that the inlet and outlet panels are not affected. Thus, the areas at these positions are equal with $A_{in} = A_{out} = 2.715 \cdot 10^{-2}\, m^2$.

The Mach number depends on the expansion ratio, the ratio of the current area to the area of the throat. Using the equation

$$\varepsilon = \frac{A}{A^*} = \frac{1}{M}\left(\frac{2}{\gamma+1}\left(1+\frac{\gamma-1}{2}M^2\right)\right)^{\frac{\gamma+1}{2(\gamma-1)}} \qquad (1)$$

the Mach number at the entry and exit planes can be computed. If a displacement of $\delta = 0.5$ is assumed the area of the throat is equal to $A^* = 2.172 \cdot 10^{-2}\, m^2$, the related expansion ratio is $\varepsilon = 1.25$. By solving Eqn. (1) with $\gamma = 1.4$ the Mach numbers for the entry and the exit plane are $M_{in,th} = 0.55$ and $M_{out,th} =$

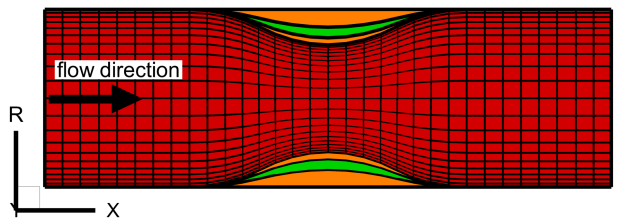

Figure 5. Mesh And Geometry For Different Displacements Of The Nozzle.

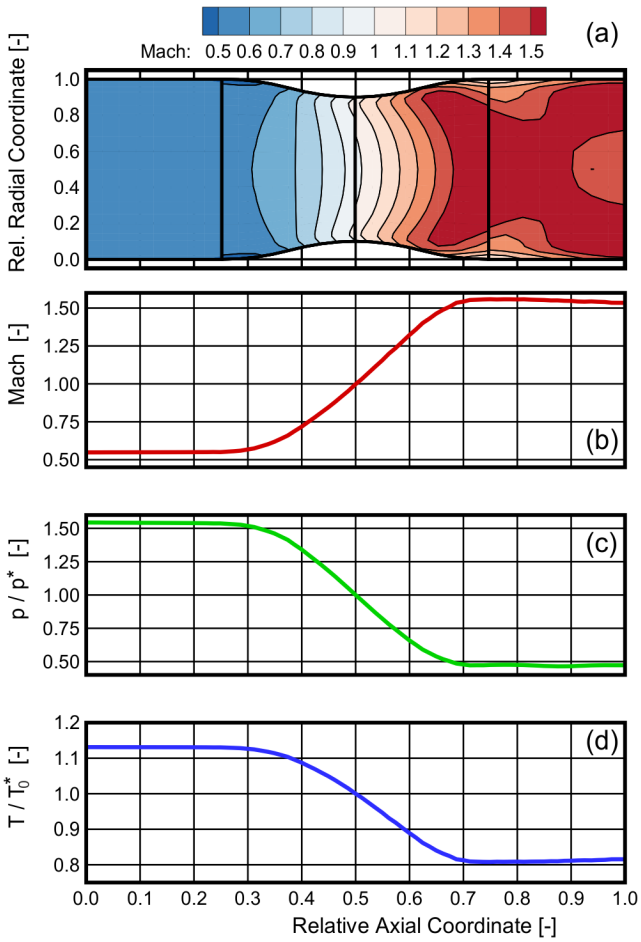

Figure 6. Results For The Nozzle With A Displacement Of $\delta = 0.5$: (a) Mach Number Contour Plot, (b) Mach Number Meanline, (c) Pressure Meanline, (d) Temperature Meanline.

1.60 respectively.

For all calculations an axial flow field is set at the inlet boundary condition with average values of the absolute total pressure of $p_{tot,abs} = 160,000\,Pa$ and the absolute total temperature of $T_{tot,abs} = 372\,K$. At the exit boundary the initial static pressure with a value of $p = 2,500\,Pa$ is chosen so low that the flow leaves the control volume supercritically.

At first a steady state computation is done using the nozzle with a displacement of $\delta = 0.5$. The results are shown in Fig. 6. The contour plots of the Mach number in Fig. 6a and its meanline in Fig. 6b show that the Mach number rises throughout the flow field and reaches the critical value in the throat. TRACE predicts a Mach number at the entry of $M_{in,CFD} = 0.55$ and at the exit of $M_{out,CFD} = 1.54$. These results correspond very well with the theoretically computed results. As the Mach number increases the values for the pressure (Fig. 6c) and the temperature (Fig. 6d) decrease. A comparison with the theoretically computed results shows a very good agreement at least for the convergent part of the nozzle. Here TRACE predicts a pressure of $p_{in,CFD} = 130,430\,Pa$ and a temperature of $T_{in,CFD} = 350.9\,K$ at the entry and the computed results are $p_{in,th} = 129,950\,Pa$ and $T_{in,th} = 350.5\,K$. For the divergent part the gap between the CFD results and the

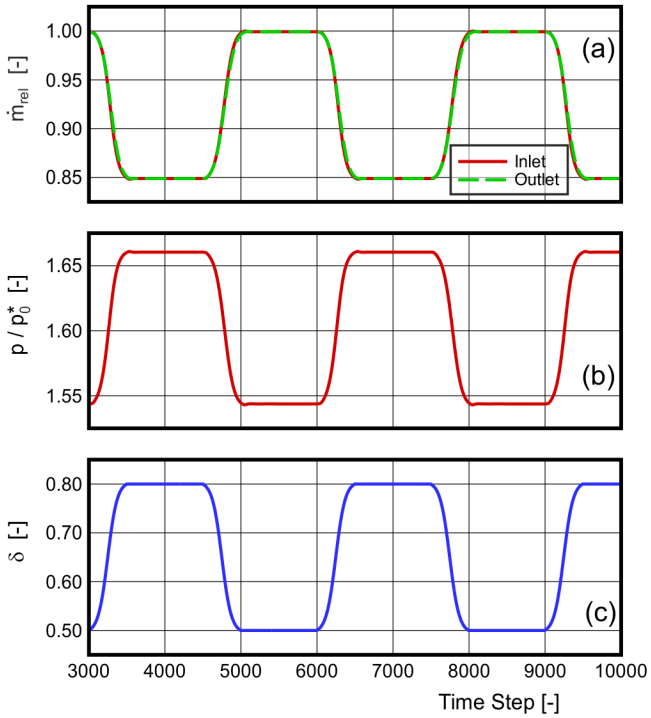

Figure 7. Progress of the Variation of the Nozzle: (a) Mass Flow, (b) Pressure and (c) Displacement.

theoretical values is slightly larger. With $p_{out,CFD} = 39,920\,Pa$ and $p_{out,th} = 37,660\,Pa$ for the static pressure at the exit as well as $T_{out,CFD} = 252.9\,K$ and $T_{out,th} = 246.0\,K$ for the temperature the results still match well.

In the final nozzle setup an unsteady calculation is set up where the displacement is varied between $\delta_{min} = 0.5$ and $\delta_{max} = 0.8$. In Fig. 5 this range is marked in green. The deformation comprises four steps. Starting from a displacement of $\delta = 0.5$ the factor is increased up to a value of $\delta = 0.8$ using a hyperbolic tangent function over 500 time steps and then it is kept constant for 1,000 time steps. After that the displacement is reduced again to a value of $\delta = 0.5$ using the inverse of the previous change and kept constant again for 1,000 time steps.

Fig. 7c shows that the displacement value follows exactly the prescribed setup. The static pressure at the duct entry switches back and forth between $p_{in,min} = 130,430\,Pa$ and $p_{in,max} = 140,280\,Pa$. These values correspond very well to the theoretical values. The progress of the mass flow (scaled with the mass flow of $\delta = 0.5$ in Fig. 7a) and the pressure (scaled with the critical pressure p_0^* for the displacement $\delta = 0.5$ in Fig. 7b) follows the change in the displacement immediately. No overshoots at the transitions are observed for the mass flow and the pressure throughout the complete computation. It proves that the implemented concept works well and can be used to control surge cycle computations.

Scaled High-Pressure Compressor

The high-pressure compressor used in this work to demonstrate the simulation of surge cycles is based on the axial compressor rig of the IST at the RWTH Aachen (Ernst,

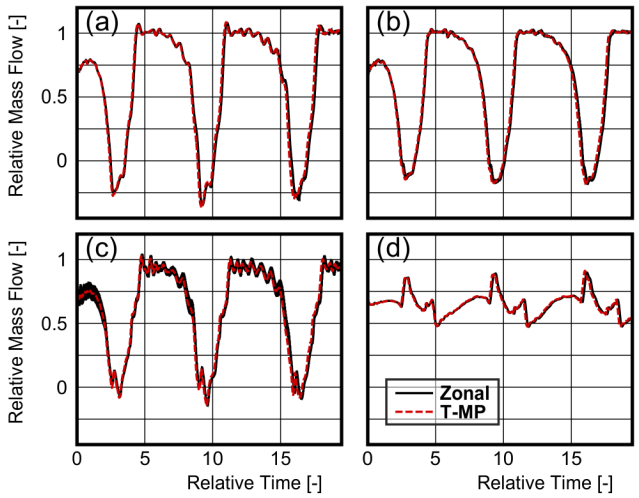

Figure 8. Progress Of Mass Flow over Time: (a) Intake - IGV, (b) IGV - R1, (c) S2 - Combustion Chamber, (d) System Exit.

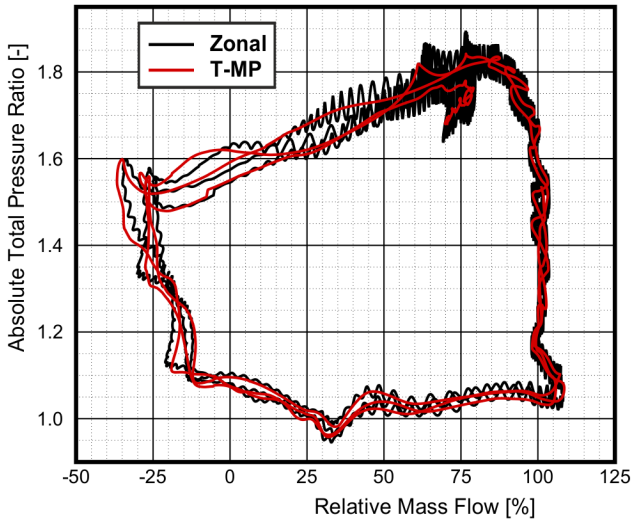

Figure 9. Hysteresis Loop Of The Compressor Surge Cycle.

2010; Gand et al., 2015) comprising two and a half stages. In this work the compressor is scaled so that all blade rows comprise 32 blades. In contrast to the real assembly a large intake is placed upstream of the compressor and a combustion chamber with the nozzle is added aft. The complete setup is shown in Fig. 1.

For the demonstration of the surge cycle the compressor itself is meshed very coarsely. The mesh in total consists of 87 structured blocks with a total of approximate 650,000 cells. The intake constitutes 25% of the total cells whereas 70% of the cells are used to mesh the compressor leaving 5% of the cells for the combustor with the attached nozzle. For the compressor the distance from the hub to casing is resolved using 32 cells for the stators and 40 cells for the rotors including 9 cells located in the tip gap region. In the core flow region an butterfly type block topology is used combined with H-type blocks at the interfaces. In the rotor tip clearance region a so-called OH-type block topology is applied.

As boundary conditions the absolute total pressure and absolute total temperature at the system inlet are applied with $p_{tot,abs} = 100,000\,Pa$ and $T_{tot,abs} = 300\,K$ respectively. For the turbulence model a turbulent intensity of $Tu = 4 \cdot 10^{-2}$ and a turbulent length scale of $l_t = 5 \cdot 10^{-4}\,m$ are selected. The static pressure at the exit of the bypass is set to $p = 99,900\,Pa$. As rotational speed $\omega = \frac{1}{t_{ref}} = 249.47\,Hz$ is chosen.

For the initial solution of the transient simulations of the surge cylce a steady computation close to the surge line is used. Here the geometry of the nozzle leads to a static pressure of $p = 150,000\,Pa$ at the interface between the combustor and the nozzle. For the unsteady simulations a second-order accurate Backward Difference Formula (BDF2) time-integration scheme (Ashcroft et al., 2013) is used with 64 time steps per blade passing frequency resulting in a resolution of 2048 time steps per rotation. Since the number of blades per blade row is constant for the entire compressor it is sufficient to resolve just one blade for each blade row if the zonal interface is used allowing to use the same mesh configuration for both interface types. In the discussion of the results the computation with the zonal interface is used as a reference for the reduced order approach with the transient mixing-plane.

For the surge cycle control the setup described in Fig. 2 is used. The displacement for the narrowest cross-section of the nozzle is varied so that pressure values at the nozzle entry vary between $p = 160,000\,Pa$ for the release phase and $p < 90,000\,Pa$. As control planes for the triggers the compressor inlet and the system exit are used. If the mass flow at the compressor inlet falls below $\dot{m} = 0\,\frac{kg}{s}$ the release phase is initiated. If the mass flow at the system exit reaches a value of $\dot{m} = 0.6875\,\dot{m}_{ref}$ without violating the previous described restriction for the release phase the throttle phase is triggered again. At the start of the computation the boundary conditions for the throttle phase are set to initiate the surge cycle.

In Fig. 8 the progress of the relative mass flow $\frac{\dot{m}}{\dot{m}_{ref}}$ for four different positions is shown for the computation with the zonal interface (Zonal) and the one with the transient mixing-plane (T-MP). The time axis is scaled with t_{ref}. In Fig. 8a it can be observed that the results at the compressor inlet for both curves evolve similarly. After a short initial phase the mass flow breaks down and falls below zero triggering the settings for the release phase. The compressor remains for approximate $4.5\,ms$ under reversed flow conditions before the flow recovers. Due to the low pressure at the system exit the mass flow rises to values above $\dot{m}_{ref}$. Since the exit pressure is reset to the higher value at $\dot{m} = 0.6875\,\dot{m}_{ref}$ the flow breaks down again and the process repeats itself. So two complete surge cycles can be counted. An FFT analysis predicts the frequency of approximate $38\,Hz$ for both interface types resulting in period lengths for the surge cycles of $0.0261\,s$ for the zonal interface and $0.0259\,s$ for the transient mixing-plane. The dwell time of the reversed flow conditions at the compressor outlet (see Fig. 8c) is significantly shorter than the one at the compressor inlet (see Fig. 8a). Here the flow becomes only briefly negative. According to Cumpsty (1989) frequencies below $10\,Hz$ are expected. But the frequency depends very much on the volumen of the combustion chamber. Therefore, the plenum seems to be too small and leads to slightly higher surge fre-

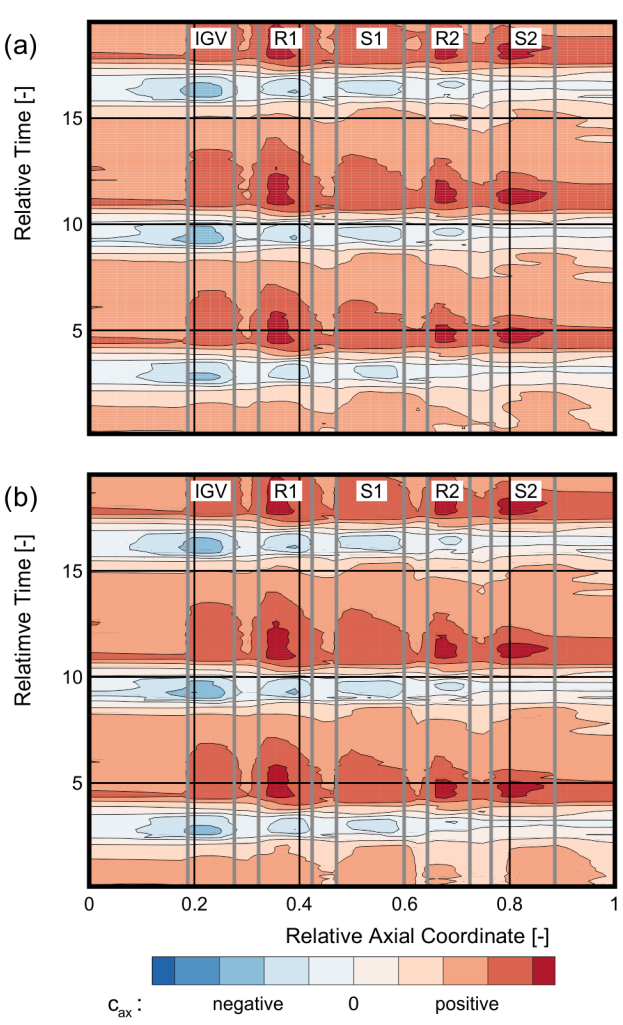

Figure 10. Axial Velocity Contour Plots For The Compressor Meanline over Time: (a) Zonal, (b) Transient Mixing-Plane.

quencies. The concept of the nozzle works as expected. The mass flow at the system exit (see Fig. 8d) is at no time negative.

For the computation with the zonal interface strong fluctuations of the mass flow are visible at the compressor outlet (see Fig. 8c). They can also be seen in the hysteresis loop of the surge cycles plotted in Fig. 9. This indicates interactions between stator 2 and the combustor volume in circumferential direction that are suppressed by the transient mixing-plane. Besides these oscillations the course of the two simulations is in good agreement for each cycle and between each other. The transient mixing-plane therefore predicts comparable results and is suitable to capture the main process for the surge cycle.

The variation of the axial velocity of the meanline of the compressor is shown over the time (scaled with t_{ref}) in Fig. 10. The leading and trailing edges of the stator vanes and the rotor blades are marked with gray lines. At $t = 2.5\,t_{ref}$ the compressor is in full reverse mode. The compressor starts to recover beginning from the outlet in upstream direction. During the phase of mass flow values above $\dot{m}_{ref}$ the highest axial velocities are observed in rotor 1. It takes nearly $2.5\,t_{ref}$ for the compressor to get into reverse mode. The blue areas indicate the regions of negative axial velocity. At first the flow seems to become negative at the inlet guide vane (IGV). As the time evolves the region expands towards the compressor outlet. But the reverse flow barely reaches the compressor outlet due to the early initiation of the pressure decrease at the exit and the comparatively small volume of the combustion chamber. The progress for the zonal interface in Fig. 10a and the one for the transient mixing-plane in Fig. 10b are qualitatively comparable.

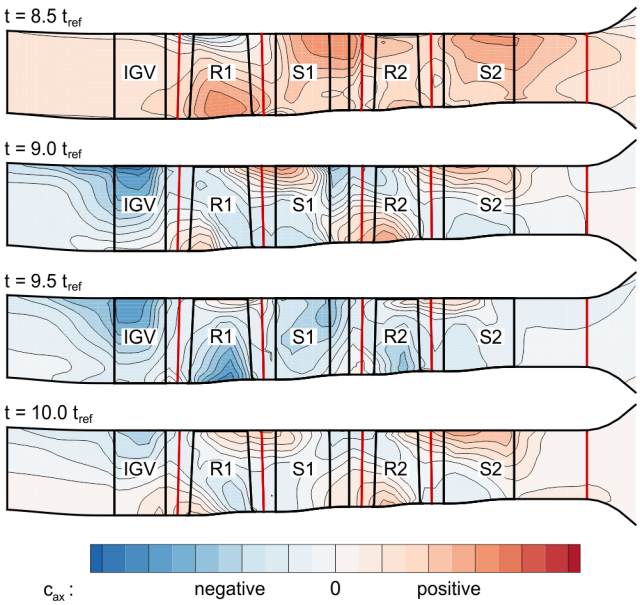

Figure 11. Meridionally Averaged Contour Plots Of The Axial Velocity At Different Times For The Solution With The Transient Mixing-Plane.

In Fig. 11 the meridionally averaged axial velocity is plotted for four different points in time using the results for the transient mixing-plane. The red lines indicate the interfaces between the blade rows whereas the black lines mark out the blades. At $t = 8.5\,t_{ref}$ negative axial velocities are observed in the tip region of rotor 1 (R1). So the actual break down starts here and not as indicated in Fig. 10 in the inlet guide vane. At $t = 9.0\,t_{ref}$ the highest negative axial velocities can be observed. But there are still areas with positive values in the hub regions of rotor 1 and rotor 2 as well as in the tip regions of stator 1 and stator 2. Later on the flow begins to recover. The positions of the vortex structures remain in the same places. The regions of positive axial velocity magnitude increase in area and magnitude until the flow recovers completely.

CONCLUSIONS

In this paper an approach to simulate compressor surge cycles has been introduced using a fully 3D setup including a large intake with a high bypass ratio and a model of the combustion chamber. Since the flow phenomenon is assumed to work primarily in axial direction the circumferential effects

can be neglected and the transient mixing-plane at the interfaces can be used. Therefore, it is sufficient to resolve one blade passage per blade row reducing the computational costs for real compressor configurations in which the numbers of blades per blade row are not proportional to each other. Two options have been presented to control the surge cycle successfully, a direct change in the pressure of the system exit and a nozzle variation placed aft of the combustion chamber.

Two basic tests have been set up to demonstrate the two key features of this approach. Using a quasi-3D duct segment the potential of the transient mixing-plane in comparison to the zonal approach and the standard mixing-plane has been shown. The nozzle concept has been proved using a convergent-divergent nozzle with a supercritical exit flow. The results show a very good agreement with the theoretical results. The modifications to the nozzle throat cause no overshoots throughout the computation making it a reliable option to control the surge cycle.

The surge cycle control has been applied successfully to a scaled high pressure compressor. Using both concepts controlling the exit pressure the expected flow cycle can be observed. It is even possible to simulate the surge cycle repeatedly. The results of the computation with the transient mixing-plane are in excellent agreement with the results of the zonal interface taken as the reference. In general the presented approach is a reliable tool to simulate surge cycles. In future works it will be applied to real compressor configurations including the comparison with experimental data.

NOMENCLATURE

Abbreviations

RANS	Reynolds-averaged Navier-Stokes
MP	mixing-plane
T-MP	unsteady mixing-plane
Zonal	zonal interface

Latin Symbols

A	area
c_{ax}	axial velocity
l_t	turbulent length scale
$\dot{m}$	mass flow rate
M	Mach number
p	pressure
r	radial coordinate
t	time
T	temperature
x, y, z	spatial coordinates

Greek Symbols

γ	heat capacity ratio
δ	displacement
ε	expansion ratio
ω	rotational speed, turbulent dissipation rate

Superscripts

$*$	critical

Subscripts

abs	absolute
CFD	CFD related value
in	inlet
max	maximum
min	minimum
out	outlet
ref	reference
th	theoretical
tot	total

ACKNOWLEDGEMENTS

This research was supported by the German Federal Ministry of Economic Affairs and Energy under the grant number 20T1515B.

REFERENCES

Ashcroft, G., Frey, C., Heitkamp, K. and Weckmüller, C. (2013), 'Advanced Numerical Methods for the Prediction of Tonal Noise in Turbomachinery — Part I: Implicit Runge-Kutta Schemes', *Journal of Turbomachinery* **136**(2).

Becker, K., Heitkamp, K. and Kügeler, E. (2010), Recent Progress In A Hybrid-Grid CFD Solver For Turbomachinery Flows, *in* 'Proceedings Fifth European Conference on Computational Fluid Dynamics ECCOMAS CFD 2010'.

Cumpsty, N. A. (1989), *Compressor Aerodynamics*, Halsted Press.

de Crécy, F., Després, G., Ngo Boum, G. and Leboeuf, F. (2013), Study Of The Aerodynamic Instabilities In An Axial Flow Compressor Using 3D-1D Codes Coupling Approach, *in* 'Proceedings of the 10th European Conference on Turbomachinery Fluid dynamics and Thermodynamics ETC10', Lappeenranta, Finland.

di Mare, L., Krishnababu, S. K., Mück, B. and Imregun, M. (2009), Aerodynamics And Aeroelasticity Of A HP Compressor During Surge And Reversed Flow, *in* 'Proceedings of the 12th International Symposium on Unsteady Aerodynamics, Aeroacoustics And Aeroelasticity of Turbomachines', number S9.4, London, UK.

Dumas, M., Duc Vo, H. and Yu, H. (2015), Post-Surge Load Prediction For Multi-Stage Compressors Via CFD Simulations, *in* 'Proceedings of ASME Turbo Expo 2015', number GT2015-42748, Montreal, Canada.

Ernst, M. (2010), Analyse von Rotor-Stator-Interaktionen und Schwingungsanregungen in einem zweistufigen Axialverdichter mit integralen Laufrädern, PhD thesis, RWTH Aachen University.

Franke, M., Röber, T., Kügeler, E. and Ashcroft, G. (2010), Turbulence Treatment in Steady and Unsteady Turbomachinery Flows, *in* 'Proceedings Fifth European Conference on Computational Fluid Dynamics ECCOMAS CFD 2010', Lisbon, Portugal.

Gand, O., Hoffmann, I., Jeschke, P. and Brignole, G. (2015), Numerical Sensitivity Analysis of the Stator Clearance on the merical Sensitivity Analysis of the Stator Clearance onFunctionality of Axial-Skewed Slot Hub Treatments, *in* 'Proceedings of International Gas Turbine Congress 2015 Tokyo', Tokyo, Japan, pp. 1271–1280.

Kügeler, E., Weber, A., Nürnberger, D. and Engel, K. (2008), Influence of blade fillets on the performance of a 15 stage gas turbine compressor, *in* 'Proceedings of ASME Turbo Expo 2008', number GT2008-50748.

Schoenenborn, H. and Breuer, T. (2011), Aeroelasticity At Reversed Flow Conditions - Part 2: Application To Compressor Surge, *in* 'Proceedings of ASME Turbo Expo 2011', number GT2011-45035, Vancouver, Canada.

Schoenenborn, H. and de Vries, M. (2012), Aeroelasticity At Reversed Flow Conditions - Part 3: Reduction Of Surge Loads By Means Of Intentional Mistuning, *in* 'Proceedings of ASME Turbo Expo 2012', number GT2012-68237, Copenhagen, Denmark.

Vahdati, M., Simpson, G. and Imregun, M. (2006), Unsteady Flow And Aeroelasticity Behaviour Of Aero-Engine Core Compressors During Rotating Stall and Surge, *in* 'Proceedings of ASME Turbo Expo 2006', number GT2006-90308, Barcelona, Spain.

Voigt, C., Frey, C. and Kersken, H.-P. (2010), Development of a generic surface mapping algorithm for fluid-structure-interaction simulations in turbomachinery, *in* 'V European Conference on Computational Fluid Dynamics ECCOMAS CFD 2010'.

Wilcox, D. C. (1988), 'Reassessment of the scale-determining equation for advanced turbulence models', *AIAA Journal* **26**(11), 1299–1310.